

Random forcing of three-dimensional homogeneous turbulence

Cite as: Physics of Fluids 11, 1880 (1999); <https://doi.org/10.1063/1.870050>

Submitted: 20 May 1998 • Accepted: 18 March 1999 • Published Online: 03 June 1999

K. Alvelius



View Online



Export Citation

ARTICLES YOU MAY BE INTERESTED IN

[Linear forcing in numerical simulations of isotropic turbulence: Physical space implementations and convergence properties](#)

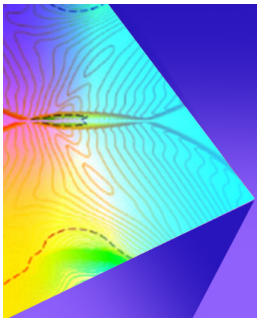
Physics of Fluids 17, 095106 (2005); <https://doi.org/10.1063/1.2047568>

[Deterministic forcing of homogeneous, isotropic turbulence](#)

Physics of Fluids 6, 1612 (1994); <https://doi.org/10.1063/1.868274>

[Forcing homogeneous turbulence in direct numerical simulation of particulate flow with interface resolution and gravity](#)

Physics of Fluids 27, 123301 (2015); <https://doi.org/10.1063/1.4936274>



Physics of Fluids
Special Topic: Shock Waves
Submit Today!

Random forcing of three-dimensional homogeneous turbulence

K. Alvelius

Department of Mechanics, KTH, SE-100 44 Stockholm, Sweden

(Received 20 May 1998; accepted 18 March 1999)

A method of using a fully random force to numerically generate statistically stationary homogeneous turbulence has been developed. The forcing is implemented in spectral space where it is concentrated at small wave numbers. Hence, the power input is introduced into the flow at large scales. The randomness in time makes the force neutral, in the sense that it does not directly correlate with any of the time scales of the turbulent flow, and it also makes the power input determined solely by the force-force correlation. This means that it is possible to generate different desirable turbulence states, such as axisymmetric turbulence, where the degree of anisotropy of the forcing can be chosen *a priori* through forcing parameters. In particular, the total amount of power input from the forcing can be set to balance a desired dissipation at a statistically stationary state. In order to only get a contribution from the force-force correlation to the input power in the discrete equations, the force is determined so that the velocity-force correlation vanishes for each Fourier mode. In direct numerical simulations (DNS) of forced isotropic turbulence, universality of the small scales is shown for the kinetic energy spectrum at different Reynolds numbers and the velocity derivative skewness obtains the value -0.5 . The forcing method is used in a large eddy simulation (LES), where it is compared with a simulation of decaying turbulence to show the importance of having a statistically stationary flow if well known inertial laws are to be recovered at moderate Reynolds numbers. © 1999 American Institute of Physics. [S1070-6631(99)01007-7]

I. INTRODUCTION

In a typical turbulent flow there is a production of turbulence kinetic energy at large scales, $\mathcal{O}(\Lambda)$, and a dissipation (destruction) of kinetic energy at small scales, $\mathcal{O}(\eta)$, where Λ and η denote macro- and Kolmogorov scale, respectively. In between there is a mean transfer of energy, the energy cascade, from large scales to small scales. The driving force, generating the turbulence, typically comes from mean velocity gradients imposed by the walls of the flow domain. These walls naturally make the turbulence inhomogeneous in the directions perpendicular to the walls. When homogeneous turbulence is considered, it is either decaying or driven by prescribed uniform velocity gradients or a volume force. In decaying turbulence, both the large scale Λ and the typical small scale η will grow with time in such a way that the Reynolds number, defined as the span $R = (\Lambda/\eta)^{3/4}$, will decrease.

In a numerical simulation of decaying turbulence, the growth of the large scale will be limited by the size of the computational domain. In a statistically stationary flow, Λ and η will be fixed at constant values during the simulation. In this paper a volume force is used to generate statistically stationary turbulence.

Several different approaches have been tried in the method of forcing homogeneous turbulence. Ghosal *et al.*¹ used a volume force of the form $\hat{\mathbf{f}}(\mathbf{k}) = \epsilon \hat{\mathbf{u}}(\mathbf{k}) / (N \hat{u}^2(\mathbf{k}))$ at each wave number \mathbf{k} in the shell $k = k_0$ containing N wave numbers, where ϵ is the dissipation rate and a caret $\hat{\cdot}$ denotes the Fourier transform. In this way they guaranteed that the production is balanced by the desired value of the dissipa-

tion. The problem with this type of force is that it is strongly correlated with the velocity field. Carati *et al.*² used the same method but tried to reduce the problem of the correlation by introducing the modification that only $N' < N$ randomly chosen wave numbers in the shell were used in the forcing.

Eswaran and Pope³ developed a method where they used a random force of the form $\hat{f}_i(\mathbf{k}, t) = (\delta_{ij} - k_i k_j / k^2) w_j(\mathbf{k}, t) \times [\Theta(\mathbf{k}) - \Theta(\mathbf{k} - \mathbf{k}_F)]$, where \mathbf{w} is a Uhlenbeck-Ornstein stochastic diffusion process, correlated over time with a chosen time scale, δ_{ij} is the Kronecker delta and Θ is the Heaviside function. However, since there is a certain time scale over which the force is correlated, the velocity-force correlation will contribute to the net forcing effect. Fureby *et al.*⁴ used this method of forcing to study subgrid-scale models for large eddy simulations. However, in their simulations they had problems in guaranteeing the same forcing for different sizes of the computations.

Siggia and Patterson⁵ tried a different approach where they kept the amplitude of the Fourier coefficients $\hat{\mathbf{u}}$ in the shell $1 \leq k \leq 2$ at a constant value, and Chasnov⁶ modified their method to only require the total energy in that wave number shell to be constant. It is difficult to say what this would physically correspond to. The method of Chasnov⁶ was also used by Sullivan *et al.*,⁷ with the difference that the energy is constant in the wave number band $k \leq K_f$, where K_f may be larger than two. She *et al.*⁸ proposed a method where the total energy in the first two wave number shells ($1 \leq k < 2$ and $2 \leq k < 3$) is kept constant in time. The ratio between the energies in the two shells is set to be consistent with the $k^{-5/3}$ law. This method has been used by Chen

*et al.*⁹ and Wang *et al.*¹⁰ to isotropically force numerical simulations.

Zhou¹¹ performed an isotropic simulation where, at each discrete time, the Fourier coefficients $\hat{\mathbf{u}}$ were multiplied with a constant at each k so that a $k^{-5/3}$ energy spectrum was obtained for all k . From this simulation he showed that the energy transfer is local in the inertial range. Overholt and Pope¹² compared the stochastic forcing of Eswaran and Pope³ with a deterministic force expressed as $\hat{\mathbf{f}}(\mathbf{k}, t) = \hat{\mathbf{u}}(\mathbf{k}, t) g_k(t) / \tau$. The function $g_k(t)$ was determined through a (mass-spring) differential equation for each wave number magnitude k . The agreement between the results from the two methods was good, whereas the deterministic method showed smaller statistical variability for most quantities.

II. RANDOM FORCING

Here we adopt the method of driving the turbulence with a random volume force. This force is implemented in spectral space, where it acts at low wave numbers with a certain prescribed distribution. It is made to be divergence free and does therefore not influence the pressure directly. The randomness in time makes it uncorrelated with the velocity field and the effect from the forcing on the velocity field is *a priori* determined by the forcing. The fact that the time scale of the forcing is separated from all time scales of the turbulent flow makes it neutral in the sense that it does not particularly enhance a certain time scale in an unknown way. Since the force is independent of the velocity field, it is possible to start a simulation from a zero velocity field, allowing the forcing to generate the turbulence, guaranteeing that the final solution is independent of the initial conditions.

A. The power input from a random force

Some effects of the random force in the Navier-Stokes (NS) equations may be studied by instead considering the simple differential equation

$$\frac{\partial}{\partial t} u_i(\mathbf{x}, t) = f_i(\mathbf{x}, t), \quad i = 1, 2, 3, \quad (1)$$

where $f_i(\mathbf{x}, t)$ is a known random force. It has the solution

$$u_i(\mathbf{x}, t) = \int_{t_n}^t f_i(\mathbf{x}, \tau) d\tau + u_i(\mathbf{x}, t_n), \quad (2)$$

where the initial value at the time t_n is assumed to be known. In the rest of the present chapter the spatial \mathbf{x} dependence is omitted in the notation for u_i and f_i . The random force is considered as white noise in time with the property

$$\langle f_k(t) f_k(\tau) \rangle = P \delta(t - \tau). \quad (3)$$

The brackets $\langle \cdots \rangle$ denote ensemble averaging over an infinite number of realizations. Define the integrated kinetic energy as $K = \overline{u_k u_k} / 2$, where the overline denotes a volume average over the whole spatial domain. The power input, i.e., the rate of change of the integrated kinetic energy, is then

$$\frac{dK}{dt} = \overline{u_k f_k} = \int_{t_n}^t \overline{f_k(t) f_k(\tau)} d\tau + \overline{f_k(t) u_k(t_n)}. \quad (4)$$

On average, only the force-force correlation contributes to the power input and (3) gives

$$\frac{d\langle K \rangle}{dt} = \int_{t_n}^t \overline{\langle f_k(t) f_k(\tau) \rangle} d\tau = P. \quad (5)$$

This means that the kinetic energy calculated from the solution of (1) will grow unlimitedly. In the NS equations the viscous dissipation will bound the growth of K , and at the statistically stationary state the dissipation will balance the production. If the relation (3) is to be satisfied, the time scale of the forcing needs to be infinitely small. In the Appendix it is shown that the effect from the forcing on the solution of the NS equations is independent of the time scale of the forcing, provided that it is much smaller than the smallest turbulence time scale.

The NS equations generally need to be discretized in order to yield a solution. A corresponding DNS algorithm for the time discretization of Eq. (1) reads

$$u_i^{n+1} = f_i^n \Delta t + u_i^n, \quad (6)$$

where the superscript n indicates that the variable is evaluated at the time t_n . The size of the time step Δt is determined by the numerical stability conditions of the NS equations and the integrated effect from the random force in Eq. (2) is approximated by a constant force during the time step. From the discrete Eq. (6), the power input averaged over one time step Δt becomes

$$\frac{K^{n+1} - K^n}{\Delta t} = \frac{1}{2} \overline{f_k^n f_k^n} \Delta t + \overline{u_k^n f_k^n} = P_1 + P_2. \quad (7)$$

Hence, there are two contributions to the total power; these are P_1 from the force-force correlation and P_2 from the velocity-force correlation, both representing the average input during the time step. The contribution P_2 should be much smaller than P_1 if the discretization is to represent the net effect from a random force with a small time scale distributed over a large number of Fourier modes, where the velocity-force correlation averaged over a finite time Δt is negligible compared to the averaged force-force correlation (see Appendix). The discretization, which makes the force constant during the period of the time step, gives a finite amplitude of the force. The force amplitude becomes, if P_1 is constant, inversely proportional to the square root of the time step ($f_i^n \sim (\Delta t)^{-1/2}$).

If, in a simulation, the random force is distributed only over a small number of Fourier modes, the volume average of the velocity-force correlation may, if no constraint is put on the discrete force, become nonzero at each discrete time. In such a case, the averaged P_2 is zero only if the average is taken over many discrete times since u_i^n does not depend on f_i^n , which is random. As the time step tends to zero, the amplitude of the forcing approaches infinity and the second term, P_2 , may become instantaneously large and has to be considered.

When the complete NS equations are solved, other terms contribute to the instantaneous power input by the forcing. However, it is shown in the Appendix that these terms are

zero on average and their instantaneous contribution decreases as the time step decreases. Hence, they may be neglected in the present analysis.

The power input by the force-force correlation can be calculated in spectral space (from now on the superscript n , indicating the discrete time, is omitted),

$$\begin{aligned} \frac{P_1}{\Delta t} &= \frac{1}{2} \frac{f_k f_k^*}{\Delta t} = \frac{1}{2} \sum \hat{f}_k(\mathbf{k}) \hat{f}_k^*(\mathbf{k}) d^3 k \\ &= 2\pi \int_0^\infty k^2 \langle \hat{f}_k \hat{f}_k^* \rangle_{\text{sph}}(k) dk \equiv \int_0^\infty F(k) dk, \end{aligned} \quad (8)$$

where $\langle \cdots \rangle_{\text{sph}}$ denotes an average over a spherical shell with radius k in Fourier space. From this we get

$$\langle \hat{f}_k \hat{f}_k^* \rangle_{\text{sph}} = \frac{F(k)}{2\pi k^2}. \quad (9)$$

The function $F(k)$ then defines the force spectrum which is prescribed.

B. Making the force divergence free

The random force is chosen to be divergence free, which in Fourier space gives the condition

$$k_k \hat{f}_k = 0. \quad (10)$$

In this way the random force does not influence the pressure directly. The random force is made divergence free by writing it in the form

$$\hat{f}_i(\mathbf{k}, t) = A_{\text{ran}}(\mathbf{k}, t) e 1_i(\mathbf{k}) + B_{\text{ran}}(\mathbf{k}, t) e 2_i(\mathbf{k}), \quad (11)$$

where $\mathbf{e}1$ and $\mathbf{e}2$ are unit vectors orthogonal to each other and to \mathbf{k} , and A_{ran} and B_{ran} are complex random numbers which remain to be determined. The relation (9) gives the condition

$$\langle A_{\text{ran}} A_{\text{ran}}^* \rangle_{\text{sph}} + \langle B_{\text{ran}} B_{\text{ran}}^* \rangle_{\text{sph}} = \frac{F(k)}{2\pi k^2}, \quad (12)$$

which is fulfilled by the choice

$$\begin{aligned} A_{\text{ran}} &= \left(\frac{F(k)}{2\pi k^2} \right)^{1/2} \exp(i\theta_1) g_A(\phi), \\ B_{\text{ran}} &= \left(\frac{F(k)}{2\pi k^2} \right)^{1/2} \exp(i\theta_2) g_B(\phi), \end{aligned} \quad (13)$$

where g_A and g_B are two real-valued functions related through $g_B^2 + g_A^2 = 1$. $\theta_1, \theta_2 \in [0, 2\pi]$ and $\phi \in [0, \pi]$ are uniformly distributed random (real) numbers generated at each wave number and discrete time level. This choice of force gives equal size of the length scales in all spatial directions. If F is made dependent on the direction of \mathbf{k} , it is possible to introduce specific length scales in the different directions.

C. Controlling the power input

Since the properties of the random force are known *a priori*, it is desirable to have a power input only through the force-force correlation, P_1 , which is controllable. If the force acts on few (low) wave numbers, P_2 may become non-zero, and if the random number generator is imperfect one may also get a net contribution to the input power from P_2 when Δt becomes small, i.e., $\langle P_2 \rangle > 0$. In order to obtain a high Reynolds number in the simulations, the force is active at low wave numbers. By using a force which is determined so that the contribution from each wave number to P_2 is zero, it is ensured that the term P_2 is zero at each time t_n . For each \mathbf{k} this gives the condition

$$\text{Real}\{A_{\text{ran}}^* \xi_1 + B_{\text{ran}}^* \xi_2\} = 0, \quad (14)$$

where $\xi_1 = \hat{u}_i e 1_i$ and $\xi_2 = \hat{u}_i e 2_i$. Introduce the angle $\psi = \theta_2 - \theta_1$, which is generated randomly with a uniform distribution on the interwall $[0, 2\pi]$. Equation (14) then gives an equation for the angle θ_1 ,

$$\tan \theta_1 = \frac{g_A(\phi) \text{Real}\{\xi_1\} + g_B(\phi) (\sin \psi \text{Imag}\{\xi_2\} + \cos \psi \text{Real}\{\xi_2\})}{-g_A(\phi) \text{Imag}\{\xi_1\} + g_B(\phi) (\sin \psi \text{Real}\{\xi_2\} - \cos \psi \text{Imag}\{\xi_2\})}. \quad (15)$$

The angle θ_2 is calculated through the definition of ψ . In this way each Fourier mode of the force has a zero correlation with the velocity field. Hence, the power input by the force is solely given by P_1 and the effect from the size of the time step is essentially eliminated.

III. THE REYNOLDS NUMBER

The characteristic length scale and velocity scale of the forcing, with which the Navier-Stokes equations are made dimensionless, are $l_* = k_f^{-1}$ and $v_* = (P/k_f)^{1/3}$. The corresponding Reynolds number is

$$R = \frac{P^{1/3} k_f^{-4/3}}{\nu}, \quad (16)$$

where ν is the kinematic viscosity. This normalization, which is only sensible to use when P is known *a priori*, gives that the dimensionless power P and forcing wave number k_f both equal unity. By putting the dissipation equal to the production by the forcing, the small (Kolmogorov) scale is estimated from

$$\eta = \frac{1}{R^{3/4} k_f}, \quad (17)$$

which is valid when a statistically stationary state has been reached. The relation (17) gives, for a specific choice of resolution, an upper limit for the Reynolds number in the simulation. The Reynolds number can, from Eq. (17), be written as the ratio between the large scale, l_* , and the small scale, η ,

$$R = (l_* / \eta)^{4/3}. \quad (18)$$

In homogeneous flows it is common to define a turbulence Reynolds number as

$$\text{Re}_T = \frac{4K^2}{\nu \epsilon}. \quad (19)$$

The turbulence Reynolds number expressed in the dimensionless turbulence kinetic energy \tilde{K} and dissipation rate $\tilde{\epsilon}$ (normalized with P and k_f) is

$$\text{Re}_T = \frac{4\tilde{K}^2}{\tilde{\epsilon}} R. \quad (20)$$

IV. SPECIFIC CHOICE

The force is given by (11), (13) and (15). The spectrum shape $F(k)$ and the functions $g_A(\phi)$ and $g_B(\phi)$ can be chosen to give the desired features of the forcing. Consider, for instance, the spectrum shape for the force as

$$F(k) = A \exp\left(-\frac{(k-k_f)^2}{c}\right). \quad (21)$$

This gives a force which is concentrated at wave number k_f with its degree of concentration determined by c . The force is limited to be active in the wave number range $k \in [k_a, k_b]$. In order to make sure that the value of the power input is equal to P , the constant A has to be chosen as

$$A = \frac{P}{\Delta t} \frac{1}{\int_{k_a}^{k_b} \exp\left(-\frac{(k-k_f)^2}{c}\right) dk}. \quad (22)$$

The components of the unit vectors describing the direction of the two force terms at each wave number \mathbf{k} are chosen as

$$e1_x = \frac{k_2}{(k_1^2 + k_2^2)^{1/2}}, \quad e1_y = -\frac{k_1}{(k_1^2 + k_2^2)^{1/2}}, \quad e1_z = 0, \quad (23)$$

$$e2_x = \frac{k_1 k_3}{k(k_1^2 + k_2^2)^{1/2}}, \quad e2_y = \frac{k_2 k_3}{k(k_1^2 + k_2^2)^{1/2}}, \quad (24)$$

$$e2_z = -\frac{(k_1^2 + k_2^2)^{1/2}}{k}.$$

With this choice, the power input in the off-diagonal elements is zero on average, and each velocity component is forced with the corresponding powers according to

$$\begin{aligned} \langle P_x \rangle &= \langle P_y \rangle \\ &= \frac{1}{2} \overline{\langle f_x f_x \rangle} \Delta t \\ &= P \left(\frac{1}{6} \langle g_B^2 \rangle + \frac{1}{2} \langle g_A^2 \rangle \right) = P \left(\frac{1}{6} + \frac{1}{3} \langle g_A^2 \rangle \right), \end{aligned} \quad (25)$$

$$\langle P_z \rangle = \frac{1}{2} \overline{\langle f_z f_z \rangle} \Delta t = P \frac{2}{3} \langle g_B^2 \rangle = P \frac{2}{3} (1 - \langle g_A^2 \rangle). \quad (26)$$

This means that the x , y and z axes become the principal axes. Since the power inputs in the x and y directions are equal, it is with this choice only possible to generate statistically axisymmetric states. The ratio between the power inputs in the different velocity components is

$$r_f = \frac{\langle P_x \rangle}{\langle P_z \rangle} = \frac{1 + 2\langle g_A^2 \rangle}{4(1 - \langle g_A^2 \rangle)}. \quad (27)$$

This ratio r_f is thus determined by the function g_A . If, e.g., $g_A = \sin(2\phi)$, $g_B = \cos(2\phi)$, the forcing becomes isotropic since $\langle g_A^2 \rangle = 1/2$ and $r_f = 1$. The choice

$$g_A(\phi) = -\frac{\tanh(b(\phi - \pi/2))}{\tanh(b\pi/2)} \quad (28)$$

presents one possibility of achieving an anisotropic forcing since we then have

$$\langle g_A^2 \rangle = \frac{1}{\tanh(b\pi/2)} \left(\frac{1}{\tanh(b\pi/2)} - \frac{2}{b\pi} \right). \quad (29)$$

Here, the degree of anisotropy can be chosen through the parameter b .

V. VALIDATION

When a stationary state has been reached in the simulation, the dissipation rate, ϵ , should equal the power input from the forcing, P . If the nonlinear terms are discarded in a numerical simulation it is also possible to predict the expected values of the kinetic energy and Reynolds stress anisotropies, $a_{ij} = R_{ij}/K - 2\delta_{ij}/3$, in terms of the forcing parameters. $R_{ij} = u_i u_j$ is the Reynolds stress tensor.

Since the forcing is implemented in Fourier space, a standard pseudospectral method with a second order mixed Crank-Nicolson and Adams-Bashforth time integration method has been used. A 3/2 dealiasing method is implemented in physical space where the nonlinear terms are calculated.

In the simulations, the discrete wave numbers are given by $\mathbf{k}(\mathbf{i}) = \mathbf{i} \mathbf{k}_f / f_{nr}$, where f_{nr} indicates which wave number shell k_f belongs to. The number f_{nr} determines how many Fourier modes are used to describe the forcing. In the present chapter all quantities are made dimensionless with l_* and v_* , which implies that the dimensionless power input and force wave number are $P = 1$ and $k_f = 1$.

A. Linear calculations

Without the nonlinear terms, the dynamic equation for the energy spectrum, E , reads

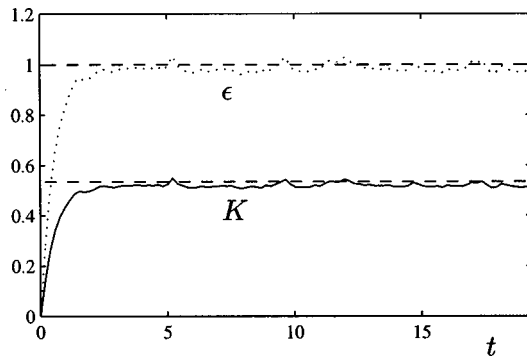


FIG. 1. The kinetic energy (solid line) and dissipation rate (dotted line) versus time in a "linear" simulation at $R=1.07$ with $\Delta t=0.02$, dashed lines: the expected stationary values.

$$\frac{dE(k)}{dt} = P(k) - \frac{2k^2}{R}E(k), \quad (30)$$

where $P(k) = \Delta t F(k)$. The total kinetic energy is integrated from the energy spectrum

$$K = \int_0^\infty E(k) dk. \quad (31)$$

When starting a simulation from a zero velocity field, E is low at the initial stage, and the last term in (30) can be neglected. This yields a linear growth of the energy spectrum equal to $t \cdot P(k)$, which is integrated to give the following expression for the total kinetic energy:

$$K = t \cdot P. \quad (32)$$

When a stationary state has been reached, the left hand side of (30) is zero and the value of the energy spectrum is determined by $E(k) = RP(k)/2k^2$, which gives

$$K = \int_{k_a}^{k_b} R \frac{P(k)}{2k^2} dk. \quad (33)$$

If the force concentration parameter, c , is small, then the major contribution to the integral comes from the wave number k_f and the stationary value of the kinetic energy can be approximated as

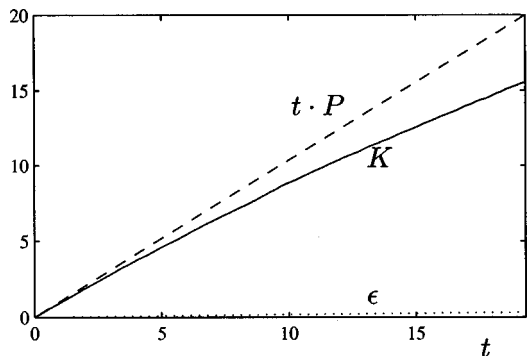


FIG. 2. The kinetic energy (solid line) and dissipation rate (dotted line) versus time in a "linear" simulation at $R=107$ with $\Delta t=0.02$; dashed line: the theoretical linear growth of K for small t .

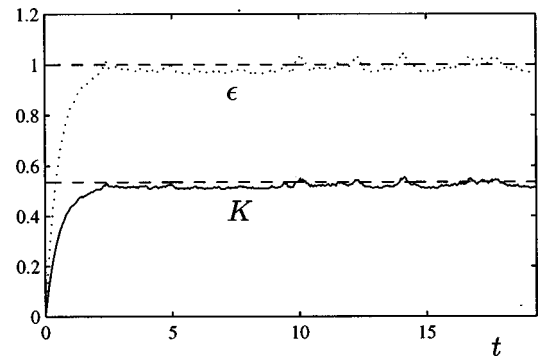


FIG. 3. The kinetic energy (solid line) and dissipation rate (dotted line) versus time in a "linear" simulation at $R=1.07$ with $\Delta t=0.005$; dashed lines: the expected stationary values.

$$K = R \frac{P}{2k_f^2}. \quad (34)$$

In Figs. 1 and 2, the kinetic energy and the dissipation are plotted for an isotropically forced 16^3 "linear" simulation with the parameter values $f_{nr}=3$, $c=0.01$, $R=1.07$ and 107 . The time step was $\Delta t=0.02$. In the $R=1.07$ case we see that the kinetic energy settles at the value 0.54 as predicted by (34), whereas in the $Re=107$ case the linear region for the increase of kinetic energy is clear in the beginning of the simulation. Another important feature of the forcing method is that if the time step is changed the results should be qualitatively unchanged. In Figs. 3 and 4 the results from a simulation with $\Delta t=0.005$ are shown. The curves are very close to those with $\Delta t=0.02$ and we may conclude that the results are insensitive to the size of the time step.

When anisotropic forcing is considered, the expected degrees of the anisotropies are

$$a_{11} = a_{22} = \frac{2}{3} \frac{r_f - 1}{2r_f + 1}, \quad a_{33} = \frac{4}{3} \frac{1 - r_f}{2r_f + 1}. \quad (35)$$

In Fig. 5 the anisotropies are shown for an anisotropically forced 16^3 "linear" simulation with $b=4$, $f_{nr}=3$, $c=0.01$, $R=1.07$ and $\Delta t=0.02$. The parameter value $b=4$ gives $r_f=4.2$ and hence the expected values of the anisotropies $a_{11} = a_{22} = -0.5a_{33} = 0.227$, which agrees well with the results

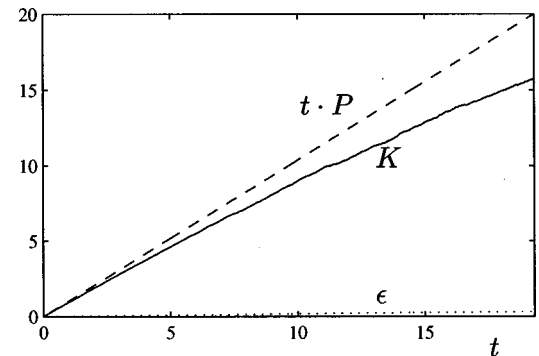


FIG. 4. The kinetic energy (solid line) and dissipation rate (dotted line) versus time in a "linear" simulation at $R=107$ with $\Delta t=0.005$; dashed line: the theoretical linear growth of K for small t .

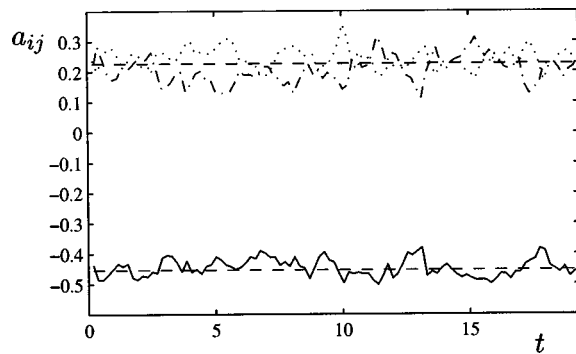


FIG. 5. Anisotropic "linear" simulation with $R=1.07$ and $b=4$. The anisotropies, a_{11} (dotted line), a_{22} (dashed-dotted line), a_{33} (solid line) and the predicted values (dashed lines).

of the simulation. The kinetic energy and the dissipation also agree well with theory (Fig. 6) as in the isotropic simulation.

B. Fully nonlinear calculations

When the complete NS equations are considered, the predictable quantities are the dissipation rate, which should equal the production in the stationary state, and the rate of change of K in the beginning of a simulation from a zero velocity field. Furthermore, the input from the velocity-force correlation and the off-diagonal components of the Reynolds stresses should be zero.

The effect of the constraint (14) is studied by carrying out two different simulations with a small time step, with and without the use of the constraint, respectively.

In Figs. 7 and 8 the kinetic energy, the dissipation rate and the Reynolds stress components are shown for isotropically forced 96^3 simulations at $R=10.7$ with the constraint (case I) and without the constraint (case II). In the simulations, the time step was $\Delta t=0.0005$ and the peak wave number for the force spectra was at $f_{nr}=3$ and $c=0.05$. This is a relatively short time step, normally used in, e.g., a 256^3 simulation, and the force is active at few wave numbers, which gives a relatively large amplitude of the force. For case II, the dissipation becomes larger than the expected

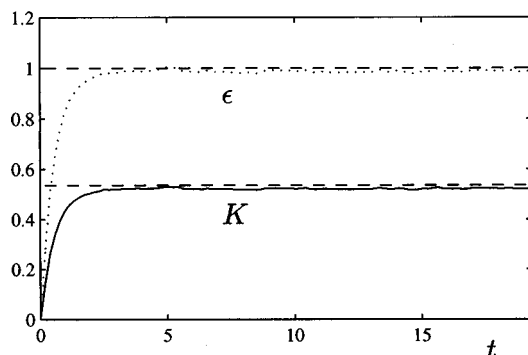


FIG. 6. Anisotropic "linear" simulation with $R=1.07$ and $b=4$. The kinetic energy (solid line), dissipation rate (dotted line) and the expected stationary values (dashed lines).

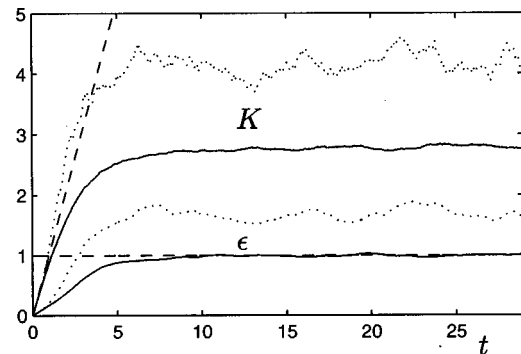


FIG. 7. K and ϵ for isotropic simulations at $R=10.7$, with the constraint (solid lines) and without the constraint (dotted lines); dashed lines: the theoretical linear growth of K and the expected stationary value of ϵ .

value of 1 and the kinetic energy grows faster than $t \cdot 1$ in the beginning of the simulation, while case I gives excellent agreement with the predictions.

The Reynolds stresses in case I attain a lower degree of anisotropy and have a much smoother variation than those of case II. Also, the off-diagonal components remain close to zero. It is apparent from these results that the use of the constraint that the velocity-force correlation should be zero significantly improves the quality of the simulation when small time steps are used. The turbulence Reynolds number becomes $Re_T \approx 320$ for case I and $Re_T \approx 430$ for case II, where the larger value of Re_T for case II is due to the extra power input through the velocity-force correlation. The Kolmogorov scale from (17) is $\eta=0.056$. The resolution in the simulations, measured by the number $k_{max}\eta=2.7$, is very high. In order to increase the Reynolds number, simulations with $k_{max}\eta=1.5$ are performed, which still is considered to be well resolved.

Isotropically forced (with the constraint) simulations with $f_{nr}=3$ and $c=0.05$ have been performed at the Reynolds numbers $R=10.7$, 23.0 and 59.0 . The highest Reynolds number simulation uses 192^3 spectral modes, while the others use 96^3 spectral modes. The time step Δt is 0.005 for the 96^3 simulations and 0.0012 for the 192^3 simulation. The behavior of the results from the $R=10.7$ simulation (Figs. 9 and 10) is the same as the results from the $R=10.7$ simula-

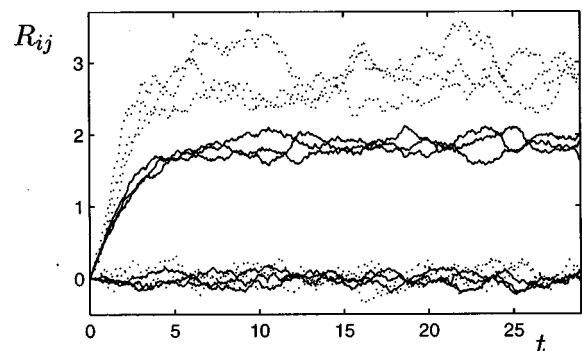


FIG. 8. The Reynolds stress components R_{ij} for isotropic simulations at $R=10.7$, with the constraint (solid lines) and without the constraint (dotted lines).

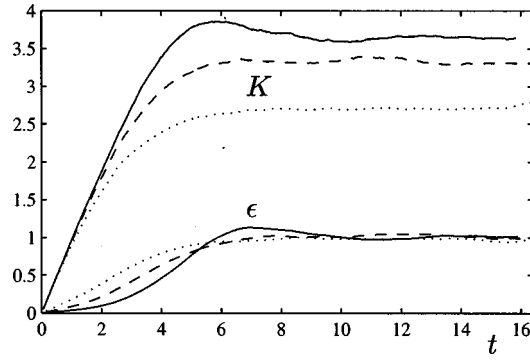


FIG. 9. The kinetic energy and dissipation rate for isotropic simulations with the constraint at $R=10.7$ (dotted lines), $R=23.0$ (dashed lines) and $R=59.0$ (solid lines).

tion with $\Delta t = 0.0005$. This illustrates the fact that the results are independent of the size of the time step also for the nonlinear simulations.

Figure 9 shows that the dissipation rate settles at the predicted value for all Reynolds numbers. The increase of ϵ in the beginning of the simulations is slower for the higher Reynolds numbers due to a wider separation between the producing and dissipative scales. This also gives a small overshoot of K for the $R=59.0$ simulation. The simulations are seen to reach a statistically stationary state in 3–4 eddy turn-over times K/ϵ . The turbulence Reynolds numbers are $Re_T = 330, 1029$ and 3079 . Since K increases with increasing R (Fig. 9), relation (20) gives that Re_T grows faster than R .

In isotropic decaying turbulence, the velocity derivative skewness

$$S_u = \frac{\left\langle \left(\frac{\partial u_1}{\partial x_1} \right)^3 \right\rangle}{\left\langle \left(\frac{\partial u_1}{\partial x_1} \right)^2 \right\rangle^{3/2}} \quad (36)$$

obtains values in the range -0.5 to -0.4 . Sullivan *et al.*⁷ and Kerr¹³ obtained values close to -0.5 in their forced simulations. Figure 10 shows the behavior of S_u for the different Reynolds numbers. For all Reynolds numbers, S_u starts from a zero value from which it decreases to -0.5 , around which it fluctuates.

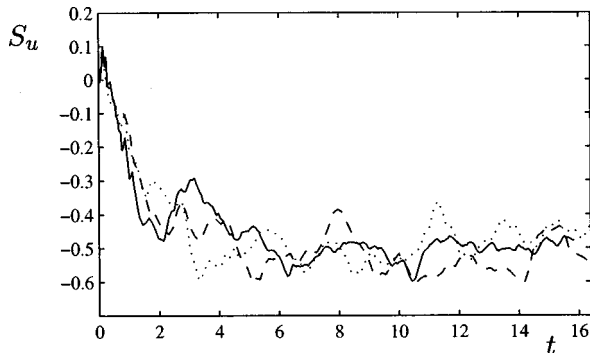


FIG. 10. The velocity derivative skewness S_u for isotropic simulations with the constraint at $R=10.7$ (dotted lines), $R=23.0$ (dashed lines) and $R=59.0$ (solid lines).

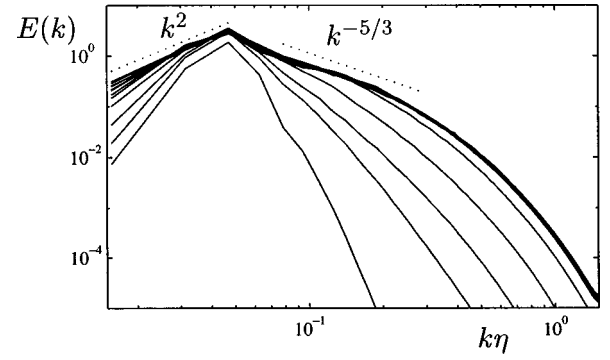


FIG. 11. The time development of the energy spectrum $E(k)$ for the $R=59.0$ simulation.

In Fig. 11 the time development of the kinetic energy spectrum is shown for the $R=59.0$ simulation. The energy spectrum obtains a peak at the forcing wave number and a slope approximately equal to k^2 for $k < k_f$. As shown by Yeung and Zhou,¹⁴ there are two possible regions with a $k^{-5/3}$ slope, where the one at lower wave numbers is associated with the inertial range. The second region, at higher wave numbers, is associated with a peak in the dissipation spectrum at $k\eta \approx 0.17$. The Reynolds number is increased to $R=101.3$ ($Re_T=5800$) in the 192³ simulation by using a force with $f_{nr}=2$. The compensated energy spectrum $E(k)\epsilon^{-2/3}k^{5/3}$ shows (Fig. 12) a universal behavior for the small scales at the different Reynolds numbers. At the lower Reynolds numbers, the forcing wave number is in the same region as the maximum dissipation and there is no $k^{-5/3}$ region. When the Reynolds number is increased, the inertial range plateau develops with a corresponding Kolmogorov constant of 1.7. The plateau at $k\eta \approx 0.17$ is, however, only marginally changed and gives a higher value 2.3. The shape of the energy spectrum at the different Reynolds numbers agrees well with the spectrum of Yeung and Zhou¹⁴ computed at a higher Reynolds number.

An anisotropically forced 96³ simulation with the constraint (14) at $R=10.7$ was carried out with $b=10, f_{nr}=3$ and $c=0.05$. The time step was $\Delta t=0.005$. In Figs. 13 and 14, the kinetic energy, the dissipation rate and the Reynolds

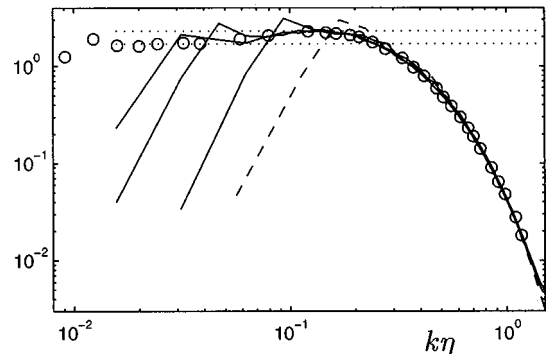


FIG. 12. The stationary state of $E(k)\epsilon^{-2/3}k^{5/3}$ for the $R=10.7$ (dashed line), $R=23.0, 59.0$ and $R=101.3$ (solid lines) simulations and the simulation by Yeung and Zhou (Ref. 14) (circles). This is compared with the values 2.3 and 1.7 (dotted lines).

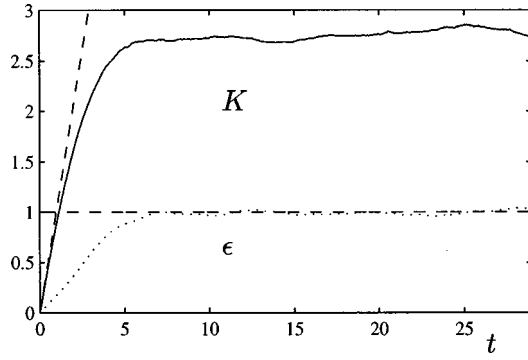


FIG. 13. The kinetic energy (solid line), the dissipation rate (dotted line) and its predicted stationary value (dashed line) for an anisotropic simulation at $R=10.7$ with $b=10$ and $f_{nr}=3$.

stresses are shown. The kinetic energy and the dissipation rate behave in the same manner as for the isotropically forced simulations, and the turbulence Reynolds number becomes $Re_T \approx 320$. The results (Fig. 14) show that the forcing puts more power into the u_1 and u_2 components compared to the u_3 component. Also, it is clear that the forcing becomes axisymmetric and the corresponding anisotropy settles approximately at $a_{33} = -2a_{11} = -2a_{22} = 0.3$.

VI. INERTIAL RANGE SIMULATIONS

The present forcing method is used in a large eddy simulation of isotropic turbulence to study well known inertial range laws for the structure function

$$B_{ij} \dots k = \langle \delta u_i \delta u_j \dots u_k \rangle, \quad (37)$$

where $\delta u_i = u_i(\mathbf{x} + \mathbf{r}) - u_i(\mathbf{x})$ is the velocity difference at two points separated by the vector \mathbf{r} . For the second and third order structure functions, Kolmogorov^{15,16} derived the relations

$$B_{II} = C(\epsilon r)^{2/3}, \quad (38)$$

$$B_{III} = -\frac{4}{5}\epsilon r, \quad (39)$$

valid for separations r in the inertial range. C is the Kolmogorov constant and “ l ” indicates the direction of the separation vector \mathbf{r} . The relation (38) can be derived from dimensional arguments while the relation (39) follows from the

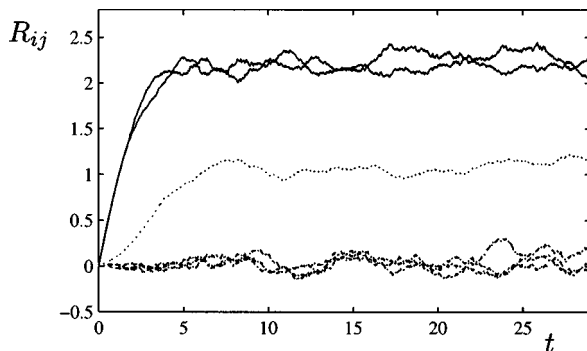


FIG. 14. The Reynolds stress components, R_{11} , R_{22} (solid lines), R_{33} (dotted line), R_{12} , R_{23} and R_{31} (dashed dotted lines) for an anisotropic simulation at $R=10.7$ with $b=10$ and $f_{nr}=3$.

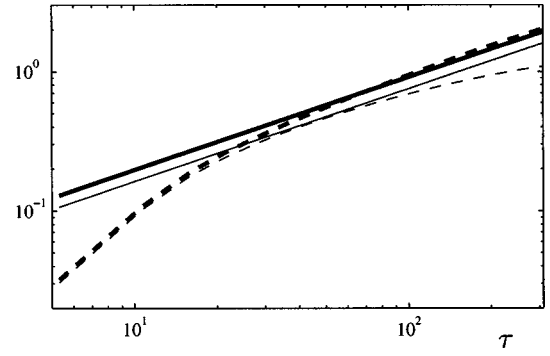


FIG. 15. The second order structure function B_{II}/ϵ from the forced (thick dashed line) and decaying (dashed line) LES compared with the curves $2.0r^{2/3}$ (thick solid line) and $1.65r^{2/3}$ (solid line).

Kolmogorov¹⁶ equation which was derived from the Navier-Stokes equations assuming statistical stationarity. In a turbulent flow which is not statistically stationary, there is in addition to the viscous term a time derivative term which needs to be small if relation (39) is to be valid. Lindborg¹⁷ derived a theoretical expression for $F = -B_{III}/(r\epsilon)$ using the $K-\epsilon$ model $\partial\epsilon/\partial t = -C_{\epsilon 2}\epsilon^2/K$ in an intermediate step

$$F(\tau) = \frac{4}{5} - C(4\tau^{-4/3} + C_*R_\lambda^{-1}\tau^{2/3}), \quad (40)$$

where $\tau = r/\eta$, $C_* = 4\sqrt{15}C_{\epsilon 2}/17$ and R_λ is the Taylor micro scale Reynolds number. From (40) it is seen that the maximum value $F = 4/5 - 3CC_*^{2/3}R_\lambda^{-2/3}$ is obtained for $\tau = (8R_\lambda/C_*)^{1/2}$. In statistically stationary turbulence the term containing C_* in Eq. (40) vanishes. Both a forced and a decaying LES are performed in order to investigate the importance of the time derivative term in the Kolmogorov equation and to compare the results with Eq. (40).

The spectral (Chollet¹⁸) model is used to describe the subgrid-scale stress tensor, together with a spherical spectral cutoff filter. The viscosity ν is set to zero in the simulations, which implies that all of the dissipation is provided by the subgrid-scale stress model. 256^3 spectral modes were used for both simulations. The forcing was performed with $f_{nr} = 2$ and $c/l_*^2 = 0.05$. After a statistically stationary state was reached, ten velocity fields were used to generate statistics. The initial field for the decaying isotropic simulation was generated with a given energy spectrum using random phases. The initial energy spectrum was given with a k^4 low wave number slope. When the initial velocity field is relaxed to a physical state, with self similar decay of the energy spectrum giving a constant value of $C_{\epsilon 2} = 1.74$, the results are taken.

Since the dissipation is modeled in the LES, the Kolmogorov scale, η , is unknown. In the decaying simulation the expressions for the maximum value of F are used to give the estimate $R_\lambda = 134$ and $\eta/l_* = 0.006$. This value of η is also used for the forced simulation since universality of the small scales is assumed and the resolved inertial range for both simulations ends at the same scale. Figure 15 shows that the forced simulation obtains a much wider region where the inertial law (38) is valid compared to the decaying simula-

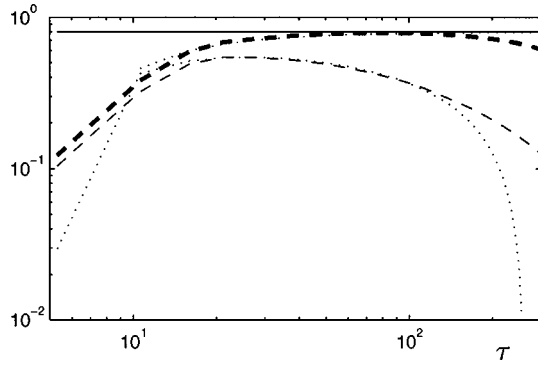


FIG. 16. The third order structure function F from the forced (thick dashed line) and decaying (dashed line) LES compared with the theory (39) by Kolmogorov (solid line) and the theory (40) with and without the time derivative term (dotted lines).

tion. The forced simulation also gives a larger value of the Kolmogorov constant $C=2.0$ compared to the decaying simulation which gives $C=1.65$. The larger value is consistent with other findings, e.g., Antonia *et al.*¹⁹ The function F from the simulations (Fig. 16) is in excellent agreement with the theory (40) in the inertial range. It is concluded that the classical relation (39) by Kolmogorov is only satisfied in the inertial range either if the Reynolds number is very high or, for moderate Reynolds numbers, if a statistically stationary state is considered.

VII. CONCLUSIONS

A stochastic volume force has been presented which gives the possibility of generating statistically stationary isotropic or anisotropic turbulence states. A constraint has been imposed which gives the discrete form of the forcing a correct behavior where only the force-force correlation contributes to the amount of input power. This also makes the effect of the force insensitive to the size of the time step in the simulations. The forcing is also insensitive to the size of simulation performed. The amount of power put into the different velocity components by the forcing can be set by force parameters. In the simulations, the stationary value of the dissipation rate equals the *a priori* set value of the production, P , and when the value of the kinetic energy, K , is low, the increase of K equals $t \cdot P$. In the linear calculation, also the total amount of kinetic energy and the degree of anisotropy agree well with the predicted values calculated from the force parameters.

In direct numerical simulations with the forcing, the universality of the small scales was shown for the compensated energy spectrum for different Reynolds numbers, and the velocity derivative skewness obtains a correct value. The forcing also proved successful in recovering classical inertial range behavior for the second and third order structure functions in a LES simulation, which was not possible in the decaying turbulence simulations.

With the forcing, the Reynolds number attainable for a given size of simulation is substantially higher than for the case of decaying turbulence. Hence, the present method, which allows an *a priori* control of the power input and flow

parameters, can be a valuable tool for the improvement of DNS as a tool for studies of homogeneous turbulence.

ACKNOWLEDGMENTS

The author wishes to thank Dr. Erik Lindborg for fruitful discussions on the present topic and professor Arne Johansson for important comments on the manuscript.

APPENDIX: THE VELOCITY-FORCE CORRELATION

The Navier-Stokes equation is written on the form

$$\frac{\partial u_i(\mathbf{x}, t)}{\partial t} = NS_i(\mathbf{x}, t) + f_i(\mathbf{x}, t), \quad (\text{A1})$$

where NS_i contains the nonlinear term, the pressure term and the viscous term. Assume that the velocity field $u_i(\mathbf{x}, t_0)$ is known (from now on only the explicit time dependence is written out). If the time difference $\delta t = t_1 - t_0$ is sufficiently small, so that the change of the term NS_i is negligible, then the velocity at the time t_1 is approximated with good accuracy by

$$u_i(t_1) = NS_i(t_0) \delta t + \int_{t_0}^{t_1} f_i(\tau) d\tau + u_i(t_0). \quad (\text{A2})$$

The effect from the forcing on the solution in (A2) enters as an integral I_i^f over the time difference δt . A simple model of a random force in the time interval $t \in [t_0, t_1]$ is

$$f_i(t) = \left(\frac{2P}{\tau_f} \right)^{1/2} w_i(n) \quad \text{if } t \in T_n = [t_0 + (n-1)\tau_f, t_0 + n\tau_f], \quad (\text{A3})$$

$$n = 1, 2, \dots, N,$$

where $\tau_f = \delta t / N$ and $w_i(n) \in [-1, 1]$ are independent “white noise” random variables, i.e., all values in the interval are equally probable for each T_n . Hence, the expectancy value and variance for each $w_i(n)$ are $E[w_i(n)] = 0$ and $V[w_i(n)] = 1/3$. With this choice of f_i , the force integral is

$$I_i^f = \int_{t_0}^{t_1} f_i(\tau) d\tau = (2\delta t P)^{1/2} \frac{1}{N^{1/2}} \sum_{n=1}^N w_i(n). \quad (\text{A4})$$

The effect on $u_i(t_1)$ from I_i^f decreases as $\delta t^{1/2}$ with smaller times δt . This guarantees that there exists a time step δt for which the approximation (A2) is correct. As N becomes large, it follows from the central limit theorem that the probability distribution of $G_i(N) = \sum_{n=1}^N w_i(n) / N^{1/2}$ approaches the normal distribution $N(0, 1/3)$ with the same expectancy value and variance as w_i . This suggests that the net effect of the forcing on $u_i(t_1)$ is independent of its time scale τ_f if N is large enough. In the simulations, the time scale $\tau_f \sim \delta t$ is smaller than the smallest time scale of the turbulence, the Kolmogorov time scale, but not small enough to give sufficient statistics in the integral.

The average power input from the force at a spatial point \mathbf{x} during the time interval T_n is

$$P^{(n)} = P w_i(n)^2 + 2P \sum_{l=1}^{n-1} w_i(l) w_i(n) + \left(\frac{2P}{\tau_f} \right)^{1/2} w_i(n) u_i(t_0) + \frac{1}{2} (2P \tau_f)^{1/2} N S_i(t_0) \left(n - \frac{1}{2} \right) w_i(n). \quad (\text{A5})$$

Average over the N intervals to get the average power input over the time δt ,

$$\begin{aligned} \frac{1}{N} \sum_{n=1}^N P^{(n)} &= P \frac{1}{N} \sum_{n=1}^N w_i(n)^2 + 2 \frac{P}{N} \sum_{n=2}^N \sum_{l=1}^{n-1} w_i(n) w_i(l) \\ &\quad + u_i(t_0) \left(\frac{2P}{\delta t} \right)^{1/2} G_i(N) + \frac{1}{2} N S_i(t_0) \\ &\quad \times (2P \delta t)^{1/2} \frac{1}{N^{3/2}} \sum_{n=1}^N \left(n - \frac{1}{2} \right) w_i(n) \\ &\equiv P_{ff1} + P_{ff2} + P_{uf1} + P_{uf2}. \end{aligned} \quad (\text{A6})$$

The law of large numbers gives that the first term, P_{ff1} , associated with the force-force correlation, rapidly converges to the value P with increasing N , and it can be shown that the double summation term, P_{ff2} , approaches zero with good certainty as N becomes large, i.e., its variance goes to zero. The variance of the term $\sum_{n=1}^N w_i(n) (n - 1/2) / N^{3/2}$ in P_{uf2} is smaller than the variance of the term $G(N)$ in P_{uf1} . The total variance of P_{uf2} is very small since it decreases with decreasing δt , while the variance of P_{uf1} can become large since it grows with decreasing δt . This suggests that the contribution from the $N S_i$ term can be neglected compared to the other terms. The time scale which determines the necessary averaging time in obtaining a small contribution from P_{uf1} is $\delta t_{\min} \sim K/P$. Although an averaged value of P_{uf1} over a longer period of time ($> \delta t_{\min}$) goes to zero with the averaging time, numerical problems associated with large instantaneous values of P_{uf1} may occur. With a Fourier representation, a volume average of the power input P_{uf1} can be written as a sum over a number of Fourier modes which is proportional to f_{nr}^2 . If the number of modes in the representation of the force is large, this average approaches zero with good certainty.

A forcing with a sufficiently small τ_f hence gives the space and time averaged production $\sum_{n=1}^N \overline{P^{(n)}} / N$ with a variance determined by f_{nr} and δt . For a given value δt , the value of f_{nr} can be chosen so that the variance becomes

arbitrarily small. In a typical DNS, the forcing is implemented at few Fourier modes in order to get a large Reynolds number. The problem of poor spatial statistics of P_{uf1} is resolved by introducing the condition that each Fourier mode of P_{uf1} is zero at each discrete time.

- ¹S. Ghosal, T. S. Lund, P. Moin, and K. Akselvoll, "A dynamic localization model for large-eddy simulation of turbulent flows," *J. Fluid Mech.* **285**, 229 (1995).
- ²D. Carati, S. Ghosal, and P. Moin, "On the representation of backscatter in dynamic localization models," *Phys. Fluids* **7**, 606 (1995).
- ³V. Eswaran and S. B. Pope, "An examination of forcing in direct numerical simulations of turbulence," *Comput. Fluids* **16**, 257 (1988).
- ⁴C. Fureby, G. Tabor, H. G. Weller, and A. D. Ghosman, "A comparative study of subgrid scale models in homogeneous isotropic turbulence," *Phys. Fluids* **9**, 1416 (1997).
- ⁵E. D. Siggia and G. S. Patterson, "Intermittency effects in a numerical simulation of stationary three-dimensional turbulence," *J. Fluid Mech.* **83**, 547 (1978).
- ⁶J. R. Chasnov, "Simulation of the Kolmogorov inertial subrange using an improved subgrid model," *Phys. Fluids A* **3**, 188 (1991).
- ⁷N. P. Sullivan, M. Shankar, and R. M. Kerr, "Deterministic forcing of homogeneous, isotropic turbulence," *Phys. Fluids* **6**, 1612 (1994).
- ⁸Z. S. She, E. Jackson, and S. A. Orzag, in *New Perspectives in Turbulence*, edited by L. Sirovich (Springer-Verlag, Berlin, 1991).
- ⁹S. Chen, G. D. Doolen, R. H. Kreichnan, and Z. S. She, "On statistical correlations between velocity increments and locally averaged dissipation in homogeneous turbulence," *Phys. Fluids A* **5**, 458 (1993).
- ¹⁰L. P. Wang, S. Chen, J. G. Brasseur, and J. C. Wyngaard, "Examination of hypotheses in the Kolmogorov refined turbulence theory through high-resolution simulations. Part 1. Velocity field," *J. Fluid Mech.* **309**, 113 (1996).
- ¹¹Y. Zhou, "Degrees of locality of energy transfer in the inertial range," *Phys. Fluids A* **5**, 1092 (1993).
- ¹²M. R. Overholt and S. B. Pope, "A deterministic forcing scheme for direct numerical simulations of turbulence," *Comput. Fluids* **17**, 11 (1998).
- ¹³M. Kerr, "Higher-order derivative correlations and the alignment of small-scale structures in isotropic numerical turbulence," *J. Fluid Mech.* **153**, 31 (1985).
- ¹⁴P. K. Yeung and Y. Zhou, "Universality of the Kolmogorov constant in numerical simulations of turbulence," *Phys. Rev. E* **56**, 1746 (1997).
- ¹⁵A. N. Kolmogorov, "The local structure of turbulence in incompressible viscous fluid for very large Reynolds numbers," *Proc. R. Soc. London, Ser. A* **434**, 9 (1941).
- ¹⁶A. N. Kolmogorov, "Dissipation of energy in the locally isotropic turbulence," *Proc. R. Soc. London, Ser. A* **434**, 15 (1941).
- ¹⁷E. Lindborg, "Correction to the four-fifths law due to variations of the dissipation," *Phys. Fluids* **11**, 510 (1999).
- ¹⁸J. P. Chollet, in *Turbulent Shears Flow IV*, edited by F. Durst and B. Launder (Springer-Verlag, Heidelberg, 1984), p. 62.
- ¹⁹R. A. Antonia, T. Zhu, F. Anselmetti, and M. Ould-Ruis, "Comparison between the sum of second-order velocity structure functions and the second-order temperature structure function," *Phys. Fluids A* **8**, 3105 (1996).